Geophysical Research Letters

RESEARCH LETTER
10.1029/2023GL103003

Plio-Pleistocene Southwest African Hydroclimate Modulated by Benguela and Indian Ocean Temperatures

Claire B. Rubbelke[1], Tripti Bhattacharya[1], Ran Feng[2], Natalie J. Burls[3], Scott Knapp[3], and Erin L. McClymont[4]

[1]Department of Earth and Environmental Sciences, Syracuse University, Syracuse, NY, USA, [2]Department of Earth Sciences, University of Connecticut, Storrs, CT, USA, [3]Atmospheric, Oceanic, and Earth Sciences, George Mason University, Fairfax, VA, USA, [4]Department of Geography, Durham University, Durham, UK

Key Points:

- Plio-Pleistocene changes in the hydrogen stable isotopic signature of leaf waxes from Southern Africa are linked to Benguela temperatures
- Higher frequency shifts in the record are likely driven by Indian Ocean temperatures via a mechanism observed in the modern
- Isotope-enabled simulations suggest that capturing this mechanism may be key to accurately simulating past and future regional hydroclimate

Supporting Information:

Supporting Information may be found in the online version of this article.

Correspondence to:

C. B. Rubbelke,
crubbelk@syr.edu

Citation:

Rubbelke, C. B., Bhattacharya, T., Feng, R., Burls, N. J., Knapp, S., & McClymont, E. L. (2023). Plio-Pleistocene Southwest African Hydroclimate modulated by Benguela and Indian Ocean temperatures. *Geophysical Research Letters*, *50*, e2023GL103003. https://doi.org/10.1029/2023GL103003

Received 25 JAN 2023
Accepted 9 SEP 2023

Author Contributions:

Conceptualization: Claire B. Rubbelke, Tripti Bhattacharya
Data curation: Claire B. Rubbelke
Formal analysis: Claire B. Rubbelke
Funding acquisition: Tripti Bhattacharya
Investigation: Claire B. Rubbelke
Methodology: Tripti Bhattacharya, Ran Feng, Natalie J. Burls, Scott Knapp
Resources: Tripti Bhattacharya
Supervision: Tripti Bhattacharya
Visualization: Claire B. Rubbelke
Writing – original draft: Claire B. Rubbelke

Abstract Future projections of southwestern African hydroclimate are highly uncertain. However, insights from past warm climates, like the Pliocene, can reveal mechanisms of future change and help benchmark models. Using leaf wax hydrogen isotopes to reconstruct precipitation (δD_p) from Namibia over the past 5 million years, we find a long-term depletion trend (−50‰). Empirical mode decomposition indicates this trend is linked to sea surface temperatures (SSTs) within the Benguela Upwelling System, but modulated by Indian Ocean SSTs on shorter timescales. The influence of SSTs on reconstructed regional hydroclimate is similar to that observed during modern Benguela Niño events, which bring extreme flooding to the region. Isotope-enabled simulations and PlioMIP2 results suggest that capturing a Benguela Niño-like state is key to accurately simulating Pliocene, and future, regional hydroclimate. This has implications for future regional climate, since an increased frequency of Benguela Niños poses risk to the ecosystems and industries in the region.

Plain Language Summary Rainfall in southwestern Africa will likely be impacted by human-caused climate change, but climate models disagree on whether the region will get wetter or drier as the planet warms. Previous studies, which used plant pollen preserved in ocean sediment, tell us that southwestern Africa was wetter during the Pliocene, a warm period approximately 5.3 to 2.5 million-years-ago, and got drier over time as Earth cooled. This drying is thought to be caused by a concurrent decrease in temperatures within the eastern South Atlantic Ocean. In this study we measure hydrogen isotopes in ancient plant matter and use statistical tools which indicate that rainfall patterns in southwestern Africa are also impacted by changes in Indian Ocean temperatures. This combined Atlantic and Indian Ocean influence is similar to events that we observe in modern times where areas of arid southwestern Africa get short bouts of very strong rainfall when the coastal waters warm. The area that gets strong rainfall depends on where the warm water occurs along the western coast and whether there's also warmer- or colder-than-normal water in the Indian Ocean. If the Pliocene ocean temperature patterns resembled these events, we may need to do further studies to determine whether they will become more common in the future.

1. Introduction

Southwestern African (SWA) rainfall encompasses diverse climatological regimes, ranging from a Mediterranean winter rainfall region in the far south, to the arid Namib desert, to tropical climates near the equator (Zhao et al., 2020). This study focuses on the arid to semi-arid regions in Namibia and Angola near the northern Benguela Upwelling System (BUS, Figure 1a), where anthropogenic climate change is already impacting dryland communities (IPCC, 2014; Stringer et al., 2009). With much of SWA already seeing an upward trend in drought and flooding (Burls et al., 2019; Muller et al., 2007; Thoithi et al., 2021), and a predicted increase in extremes (Kusangaya et al., 2014), it is imperative to understand the mechanisms driving these changes.

Thermodynamic scaling suggests that anthropogenic warming will amplify patterns of wet and dry; "wet-get-wetter, dry-get-drier" (Held & Soden, 2006). However, this simple scaling cannot account for patterns of hydroclimate change over many land regions, including SWA (Byrne & O'Gorman, 2015; Seager et al., 2010). While earth system models broadly agree that the African continent will become hotter and drier over the coming century (IPCC, 2014; Kusangaya et al., 2014), there is significant disagreement about regional hydroclimate patterns as well as timescales of hydroclimate change (Baxter et al., 2023; Burls & Fedorov, 2017; Byrne & O'Gorman, 2015;

Writing – review & editing: Claire B. Rubbelke, Tripti Bhattacharya, Ran Feng, Natalie J. Burls, Scott Knapp, Erin L. McClymont

Feng et al., 2022b; Fu et al., 2021; IPCC, 2014; Ogega et al., 2020; Seo et al., 2014; Xie et al., 2010). For southern Africa, some models indicate that current drying trends may be transient, and that long-term dynamical adjustments will compensate for initial thermodynamically-driven drying (Sniderman et al., 2019).

Past equilibrium greenhouse climate states, including the Pliocene, can serve as analogs for future climate (Burke et al., 2018). The Pliocene featured a similar-to-present continental configuration and atmospheric CO_2 concentrations that were above 400 parts per million (de la Vega et al., 2020; Haywood et al., 2020; Rae et al., 2021). Poleward amplified warming may have weakened meridional atmospheric circulation, driving a "wet-get-drier, dry-get-wetter" Pliocene hydroclimate response (Burls & Fedorov, 2017).

When forced with Pliocene boundary conditions, coupled models show substantial disagreement about SWA hydroclimate (Pontes et al., 2020). In addition, Pliocene Model Intercomparison Project (PlioMIP2) generally simulate drier conditions relative to present-day in Namibia and Angola (Figure S8 in Supporting Information S1), at odds with available proxy evidence. Palynological evidence from ODP Sites 1081 and 1082 (in the BUS) show that a long term aridification in SWA began during the late Miocene/early Pliocene (8–5 Ma), initiating a shift from mesic shrubland and woodland to savannah grasslands (Hoetzel et al., 2013, 2015; Zhao et al., 2020). After 5 Ma, and again after 2 Ma, progressive aridification increased semi-desert and desert taxa (Dupont, 2006; Dupont et al., 2005; Etourneau et al., 2009; Marlow et al., 2000). Long-term aridification has been attributed to cooling of sea surface temperatures (SSTs) in the BUS (Dupont, 2006; Dupont et al., 2005; Hoetzel et al., 2013, 2015). This evidence suggests that land regions near the BUS were *wetter* in the Pliocene compared to the late Pleistocene, in contrast with PlioMIP2 models' simulation of drier-than-present conditions (Pontes et al., 2020). Understanding the source of proxy-model and intermodel disagreement surrounding Pliocene hydroclimate in southwestern Africa is key to honing projections of water resources in this semi-arid region.

Additional proxy records can reveal causes of proxy-model disagreement. In other regions of Africa, Plio-Pleistocene records have revealed details of how orbital and greenhouse gas forcing shaped local hydroclimate (Kuechler et al., 2018; Lupien et al., 2021, 2022). However, there are relatively few sub-million year hydroclimate records spanning the Plio-Pleistocene in SWA (Cohen et al., 2022)—isotopic records of hydroclimate spanning this interval are particularly sparse. The hydrogen isotopic ratio of long-chain leaf waxes (δD_{wax}) in sedimentary archives shows a strong relationship with the isotopic composition of precipitation (δD_p) (Diefendorf & Freimuth, 2017; Feakins, 2013; Feakins & Sessions, 2010; Feakins et al., 2005; Gao et al., 2014; Hemingway et al., 2019; Herrmann et al., 2017; Inglis et al., 2022; Liu et al., 2023; Sachse et al., 2004, 2012; Sessions & Hayes, 2005; Smith & Freeman, 2006; Vogts et al., 2016). Changes in δD_p can reveal overall changes in past aridity, but may also reveal additional processes including temperature, atmospheric circulation and vapor source, as well as the characteristics of past precipitation (e.g., convective vs. stratiform, seasonality) (Belz et al., 2020; Bhattacharya et al., 2022; Collins et al., 2013; Dupont et al., 2013; Feakins, 2013; Garelick et al., 2021; Konecky et al., 2011; Kuechler et al., 2018; Li et al., 2017; Lupien et al., 2022; Taylor et al., 2021; Tierney et al., 2017; Vogts et al., 2016). Information from leaf wax reconstructions of δD_p can therefore provide unique insights on past reorganizations of regional atmospheric circulation.

Here, we present a new leaf wax hydroclimate record from ODP 1081, focusing on the early Pliocene through the late Pleistocene. We compare these data to SST records from the BUS and Indian Ocean to explore the physical mechanisms driving the signal in our leaf wax record. Using observational data and model simulations, we highlight the relevance of this mechanism for understanding Pliocene proxy-model disagreement in SWA, and implications for understanding present-day climate change.

2. Methods

2.1. Regional Setting

ODP 1081 (19°37.1818′S, 11°19.1598′E) is located at the northern boundary of the BUS (Figure 1a). Terrigenous sediments are sourced from the Cuvelai and Kunene watersheds via the Kunene River (Hipondoka, 2005), and via aeolian deposition (Dupont & Wyputta, 2003). SWA hydroclimate is moderated by the South Atlantic and Indian Ocean anticyclones (Hutchings et al., 2009). Southeast trade winds drive coastal upwelling, which is enhanced in the northern BUS seasonally by a transient low-level coastal jet (Nicholson, 2010). The cold waters of the BUS, the coastal jet, and dry descending air contribute to aridity (Eckardt et al., 2013; Kaseke et al., 2016; Nicholson, 2010; Zhao et al., 2020). The northern boundary of the BUS occurs at the Angola-Benguela Front (~17°S), and is sensitive to the seasonal displacement of the South Atlantic anticyclone (Rouault et al., 2007).

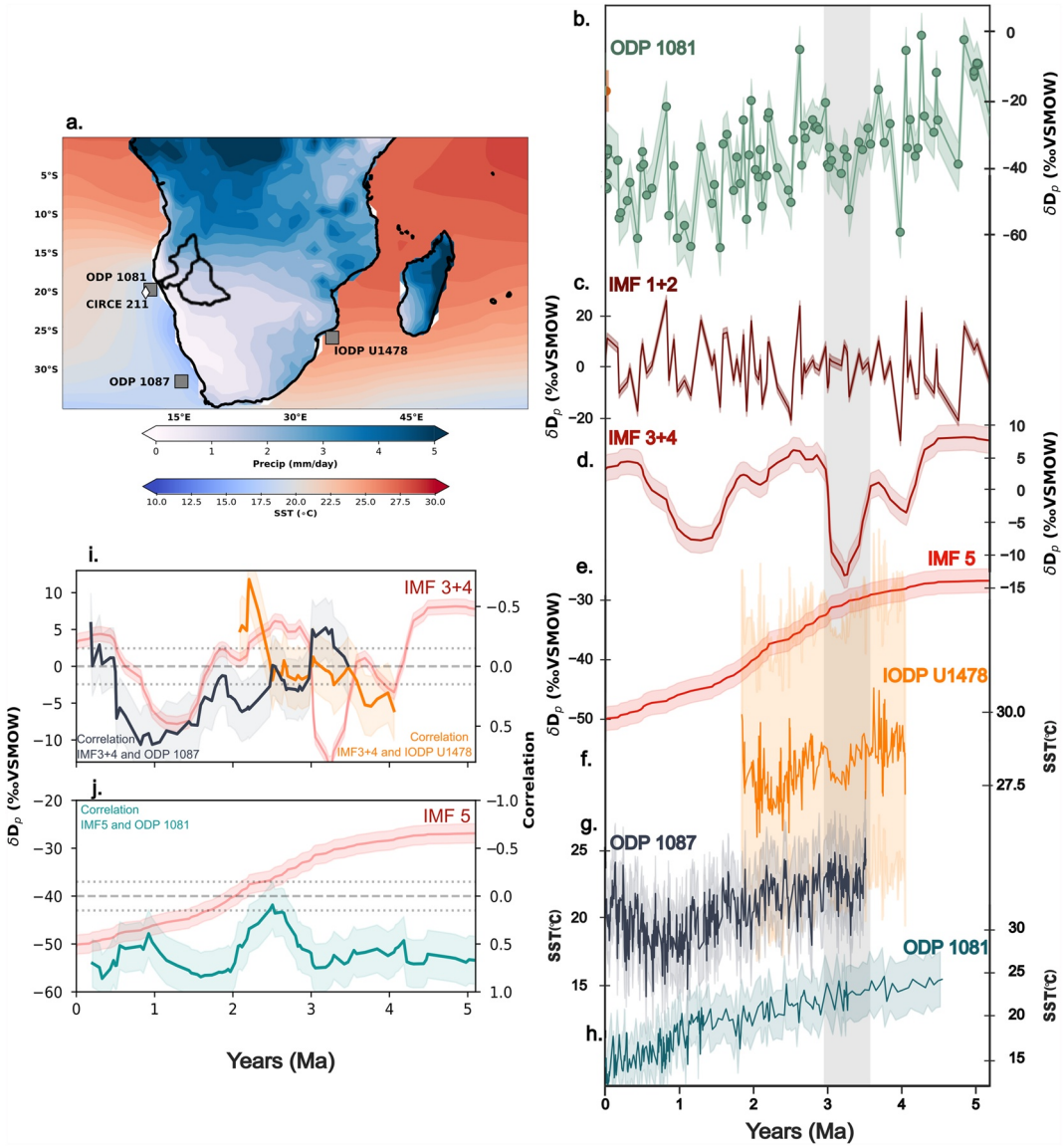

Figure 1. (a) Modern climatology of the South Africa from reanalysis data. Markers show the location of ODP and IODP drill sites in the Benguela Upwelling System and Agulhas Current (gray squares) and coretop samples (white diamond). Black outlines Kunene in the north and Cuvelai in the south drainage basins. (b) The δD_p record from ODP 1081 (green, this study) and CIRCE coretop 211 (tan, this study), (c) sum of the first two IMFs, (d)sum of the third and fourth intrinsic mode function (IMF), and (e) fifth IMF. (f) TEX_{86} derived sea surface temperature (SST) record for IODP U1478 (Taylor et al., 2021), (g) alkenone derived SST for ODP 1087 (Petrick et al., 2015), and (h) alkenone derived SST for ODP 1081 (Rosell-Melé et al., 2014). The gray bar highlights the mid-Piacenzian warm period. (i) Running correlation between IMF3 + 4 and the U1478 SST (orange line) as well as 1087 SST (gray line), overlain with IMF3 + 4 timeseries. (j) Running correlation between IMF5 and the 1081 SST (teal), overlain with IMF5 timeseries. The dashed line marks 0 correlation, and the dotted lines mark ±95% significance bounds for correlation coefficient (note that positive is down on *y* axis).

During austral summer (December-January-February, DJF), climatological low-level moisture transport over Southern Africa is from the Indian Ocean, bringing relatively deuterium enriched (−60 to 0‰) vapor to the continental interior (Figure S1 in Supporting Information S1) (Good et al., 2015; Reason, 2001; Reason, Landman, & Tennant, 2006). This moisture becomes progressively depleted in deuterium as it travels over the continent and rains out before it meets the Namib Desert (Kaseke et al., 2016).

2.2. Proxy Data

2.2.1. Sample Preparation and Analytical Methods

Samples were lyophilized and homogenized. Total lipid extracts (TLEs) were collected using an Accelerated Solvent Extraction (ASE 350, Dionex) system. *n*-Alkanes were separated from the TLEs with hexane over a column of 5% deactivated silica gel. *n*-Alkanes were quantified on a Thermo Scientific Trace 1310 GC with a flame ionization detector and a programmable temperature-vapourization inlet fitted with an Agilent 30-m DB5 column and H_2 as a carrier gas. *n*-Alkane concentrations were determined by comparing to peak areas of a known quantity of internal standard (5-α androstane) using the MATLAB package ORIGaMI (Fleming & Tierney, 2016). We calculated the carbon preference index (CPI) and average chain length (ACL) of our leaf waxes. CPI values averaged 3.364 ± 0.44 (1-σ), indicating terrestrial rather than petrogenic inputs (Jeng, 2006), and ACL (Mean ACL = 29.6 ± 1.2 (1-σ)) showed very little variation over our record (Figure S2 in Supporting Information S1). Because of high concentrations of C_{31} (mean 40 ± 7.24 ng/g (1-σ)), and because previous studies from SWA have focused on the C_{31} alkane (e.g., Dupont et al., 2013), we report isotopic results from this chain length.

Compound-specific hydrogen and carbon isotopes were measured for the C_{31} alkanes using a Thermo Scientific Trace 1310 Gas Chromatograph coupled via an Isolink device with combustion (carbon) and pyrolysis (hydrogen) furnace to a Delta V Plus isotope ratio mass spectrometer (GC-IRMS). Reference H_2 and CO_2 gases calibrated to an *n*-alkane standard (A7 mix provided by Arndt Schimmelmann at Indiana University) provided references for each analysis. Injections of A7 mix and an internal standard were used to monitor instrument drift. The H_3 factor was an average of 4.703 ppm/mV over a range of 1–8 V. Samples were run in triplicate for δD to obtain a precision better than 3‰, and duplicate or triplicate for $\delta^{13}C_{wax}$ to obtain a precision better than 0.2‰. Samples that did not meet these thresholds were excluded from the results; the average standard deviation of included hydrogen and carbon measurements were 1.81 and 0.104, respectively.

2.2.2. Inferring δD of Precipitation From Leaf Waxes

The hydrogen isotopic signature of leaf wax compounds, δD_{wax},is offset from the hydrogen isotopic signature of the environmental source waters, generally assumed to be precipitation (δD_p). This apparent fractionation, ε_{p-wax}, integrates isotopic offsets related to evapotranspiration and wax biosynthesis. ε_{p-wax} varies across plant clades (Collins et al., 2013; Freimuth et al., 2017; Griepentrog et al., 2019; Inglis et al., 2022; Sachse et al., 2012; Tipple et al., 2015). Waxes synthesized by graminoids tend to have a larger ε_{p-w} than those of eudicots (Gao et al., 2014; Sachse et al., 2012; Vogts et al., 2016). Inferring δD_p requires independent knowledge of the proportion of graminoids on the landscape. To infer the grass proportions, we use measurements of $\delta^{13}C_{wax}$, since C_4 grasses have a distinct carbon isotopic signature. Then, we use modern empirically derived constraints on ε_{p-wax} from grasses and eudicots (Freimuth et al., 2017; Garcin et al., 2014; Sachse et al., 2012) to calculate an appropriate ε value. Within a Bayesian framework, we weighε by the proportion of graminoids inferred from $\delta^{13}C_{wax}$ in a sample, thereby accounting for the variable fractionation between graminoids and eudicots. We then use this new weighted ε to infer δD_p from δD_{wax} (see method and Figure S2 in Supporting Information S1).

This approach has been widely applied to infer δD_p from leaf wax δD in Africa (e.g., Garelick et al., 2021; Lupien et al., 2022; Tierney et al., 2017). We also used an alternate approach, using pollen data from ODP 1081 (Hoetzel et al., 2013) to infer the proportion of graminoids on the landscape, similar to the approach in Feakins (2013). A Student's *t*-test showed that these methods do not yield significantly different results ($p > 0.05$), since both $\delta^{13}C_{wax}$ data and pollen records imply very modest changes in the percentage of graminoids between 4 Ma and the present (Dupont et al., 2005). Because our $\delta^{13}C_{wax}$ record is higher resolution, we use $\delta^{13}C_{wax}$ measurements to correct the δD record (Figure S2 in Supporting Information S1). For brevity, subsequent uses of "δD_p" refers to C_{31} alkane-inferred values of δD of precipitation.

2.3. Model Data

We analyze pre-industrial and Pliocene climate simulations of the isotope-enabled Community Atmosphere Model version 5 (iCAM5) (Nusbaumer et al., 2017). The preindustrial control simulation features fixed SSTs and sea ice derived from the 1970–1980 climatological average (Hurrell et al., 2008). Simulated preindustrial δD_p patterns agree with the modern SWA isoscape (Kaseke et al., 2016; Knapp et al., 2022b). The second is an early (5–4 Ma) "Pliocene-like" simulation, with SSTs and sea ice fields taken from an idealized experiment

with perturbed cloud albedo (Burls & Fedorov, 2014). All other boundary conditions, including paleogeography, are set to modern values, allowing us to isolate the influence of SST patterns on regional hydroclimate (Knapp et al., 2022b).

3. Results and Discussion

3.1. Late Cenozoic Southwest African Hydroclimate and Vegetation

The leaf wax carbon and hydrogen isotopic data from ODP 1081 extends from 5 Ma to present and complements previously published Cenozoic southern African climate records (Figure S3 in Supporting Information S1). Our leaf wax $\delta^{13}C_{wax}$ record overlaps in range with the lower resolution Mio-Pliocene record presented in Hoetzel et al. (2013), and confirms a long-term shift toward more enriched values of $\delta^{13}C_{wax}$ over the late Cenozoic. $\delta^{13}C_{wax}$ values of the C_{31} alkanes ranged from −27.5 to −22.5‰ VPDB, with increasing values from ∼3.5 to 1.8 Ma. From ∼1.8 Ma to present, $\delta^{13}C_{wax}$ values remain around −22.5‰ VPDB. This appears at odds with pollen records indicating a decline in grass abundance after 4.5 Ma. However, Dupont et al. (2013) and Hoetzel et al. (2013) suggest that a higher C_4 contribution may derive from plant waxes from desert taxa that use C_4 or CAM metabolism but are underrepresented in the pollen record. However, our pollen-based and carbon isotope-based vegetation corrections do not yield statistically significantly different results for δD_p.

The leaf wax-inferred δD_p record shows a long term depletion trend, with more positive values in the Pliocene (Figure 1b). However, the record is also more variable in this interval than in the late Pleistocene, with values ranging from approximately −5 to −60‰ VSMOW during the early to mid-Pliocene (∼5–3.3 Ma). We do not anticipate that these trends are the result of glacial/interglacial variability, since global and local records point to a more muted glacial-interglacial variability in the Pliocene compared to the Pleistocene (Dupont et al., 2013; Etourneau et al., 2009; Lisiecki & Raymo, 2005). In addition, the long-term depletion trend in deuterium is superimposed on large, sub-million year fluctuations in δD_p (Figure 1b). Between 3.5 and 2.9 Ma, values of δD_p decrease to roughly −40‰, before increasing to more enriched values between 2.9 and 2.7 Ma. A similar reversal to more depleted values occurs around 1 Ma, with lowest values of −60‰ VSMOW. δD_p inferred from a nearby coretop, which yields a median value of -16.32 ± 8.5‰VSMOW, is consistent with modern precipitation isotopes (Kaseke et al., 2016).

In the modern climatology, δD_p is enriched in coastal Namibia relative to the interior of the continent, as a result of sub-cloud evaporation processes in an extremely arid environment (Kaseke et al., 2016). Water vapor δD exhibits a progressive depletion moving from east to west, reflecting the progressive rainout of Indian Ocean moisture (Figure S1 in Supporting Information S1). At first glance, a more enriched mid-Pliocene δD_p could reflect an intensification of sub-cloud evaporative processes as a result of enhanced Pliocene aridity. In addition, the traditional "amount effect" would suggest that a Pliocene enriched hydrogen isotopic signature indicates drier conditions. However, these interpretations are at odds with palynological and carbon isotope evidence that points to higher coverage of mesic taxa in the Pliocene, implying greater Pliocene moisture availability (Dupont, 2006; Dupont et al., 2005, 2013; Hoetzel et al., 2013, 2015).

Instead, the synergy between our δD_p records and Pliocene climate simulations imply that a more enriched Pliocene δD_p signature reflects changes in moisture source, as well as an increased proportion of convective rainfall. Specifically, a more positive hydrogen isotopic signature of δD_p may reflect a greater proportion of vapor from the tropical Atlantic (Figures 3c and 3d). An increased contribution to rainfall from local evaporation from a warmer southeastern Atlantic would result in a more enriched signature compared to vapor from the Indian Ocean that has undergone significant distillation during cross-continental transport. A higher proportion of deep convective rainfall, supplied by local and tropical Atlantic moisture sources, would also have a more enriched isotopic signature compared to more stratiform precipitation sources (Aggarwal et al., 2016; Maupin et al., 2021).

A shift in vapor source is consistent with isotope-enabled regional model simulations that show that a shift to Atlantic-sourced vapor drives increases in δD_p in SWA (Arnault et al., 2022). It also builds upon the interpretation of Dupont et al. (2013), who suggest that a progressive shift to more Indian Ocean sourced moisture occurred between 7 and 4.5 Ma, resulting in progressive depletion of SWA δD_p. Our record therefore suggests a Plio-Pleistocene shift toward an Indian Ocean vapor source, super-imposed with large sub-million year fluctuations. If this interpretation is correct, we would expect to see a strong correlation between our leaf wax inferred δD_p record and BUS and the Indian Ocean SSTs.

3.2. Empirical Mode Decomposition and Regional SST Controls on Hydroclimate

The long-term depletion trend of δD_p values seems to agree with the long-term aridification inferred from paleobotanical evidence, and aligns well with the long-term cooling seen in the BUS. However, the sub-million year fluctuations in δD_p imply a more complex dynamic may be at work over intervals greater than orbital-scale processes. To more clearly elucidate different timescales of variability in our record, we employed an empirical mode decomposition (EMD). EMD utilizes a sift algorithm to isolate the fastest (higher frequency) dynamics in a time-series by iteratively sifting out slower (lower frequency) dynamics; the algorithm continues to sift out lower frequency signals until a non-oscillatory signal remains (Quinn et al., 2021). The relative magnitude of each isolated signal, or intrinsic mode function (IMF), is calculated as part of this process (Huang et al., 1998; Quinn et al., 2021; Wu & Huang, 2004). The sum of all decomposed modes yields the original signal (Quinn et al., 2021) (see Supporting Information S1 Text).

Our sampling interval does not permit the clear resolution of Milankovich-scale periodicities - a Lomb-Scargle power spectrum analysis does not indicate significant orbital variability at the current resolution (Figure S4 in Supporting Information S1) (Astropy Collaboration et al., 2022); we thus sum IMFs 1 and 2 for display (Figure 1c). These modes capture higher frequency variations in our record (Figure S5 in Supporting Information S1). Higher-resolution records are needed to probe orbital-scale hydroclimate variations, as have been done in other settings (Kuechler et al., 2018).

Our record most clearly resolves sub-million year timescales. The sum of IMFs 3 and 4 (Figure 1d) reflects sub-million year fluctuations, and captures decreases δD_p between 3.5 and 2.9 Ma and at 1 Ma. IMF 5 (Figure 1e) captures a long-term trend toward values more depleted in deuterium. The magnitude of IMFs 3 and 4 is on the order of 15‰ and is similar to the 20‰ depletion trend captured by IMF 5, implying that sub-million year variability drives a similar magnitude of change in δD_p as the long-term trend related to aridification.

Contrasting these IMFs with SST proxies provide clues about the drivers of Plio-Pleistocene hydroclimate change in SWA. The long-term depletion trend captured by IMF 5 has a statistically significant positive correlation with BUS SSTs over the entire record (Figures 1h and 1j). This is consistent with previous interpretations that BUS cooling drove a decrease in convective activity and a shift to more Indian Ocean-sourced vapor, both of which would result in progressive depletion of δD_p (Dupont et al., 2013; Hoetzel et al., 2013). However, a new feature of our record is the presence of strong sub-million year scale variations, which our EMD analysis indicates are of a similar magnitude to the long-term drying trend. Notably, IMF3 + 4 exhibits non-stationary correlations with Indian Ocean SSTs. These modes are significantly positively correlated with the TEX_{86}-based SST record from IODP U1478 between 4 and 3.5 Ma, prior to an interval between 3.5 and 2.9 Ma when we observe depleted δD_p values at 1081 and cooler SSTs at U1478 (Figures 1f and 1i) (Taylor et al., 2021). In addition, IMF3 + 4 exhibits a statistically significant positive correlation with an alkenone-based SST record from ODP 1087, especially between 1.5 and 1 Ma (Petrick et al., 2015), a cooling interval in this record. This site is influenced by Atlantic and Indian Ocean processes via the Agulhas leakage (Figures 1g and 1i). IMF3 + 4 therefore indicates that during certain intervals, δD_p at 1081 is influenced by Indian Ocean SSTs. This suggests the possibility that SST gradients between the Indian and South Atlantic Ocean could drive sub-million year variations in regional hydroclimate.

3.3. Modern Impact of BUS and Indian Ocean SST on Local Hydroclimate

While our correlation analysis is intriguing, further evidence is needed to reveal the dynamical mechanisms by which BUS and Indian Ocean temperatures drive hydroclimate changes over Namibia. We first analyze the observational record. In the mean summertime climatology, easterly moisture flux transports water vapor from the Indian Ocean over the continent. This moisture rains out and becomes deuterium-depleted over the southwestern part of the continent. When these winds reach the Namib Desert and Angolan coast, vapor is limited, and dry berg-type winds contribute to coastal aridity (Tyson & Seely, 1980). This arid hydroclimate state is reversed during Benguela warming events, or Benguela Niño s (Bachèlery et al., 2020; Florenchie et al., 2003; Reason, Florenchie, et al., 2006; Rouault et al., 2003, 2007), which feature SST anomalies greater than those induced by anthropogenic warming. The Benguela Niño s are associated with extreme convective precipitation in Namibia and Angola (Florenchie et al., 2003; Rouault et al., 2003, 2007). The location and intensity of extreme precipitation during Benguela Niño s is modulated by Indian Ocean SSTs (Rouault et al., 2003). This is illustrated by comparing two Benguela Niño events: the 1984 Benguela Niño event is associated with positive

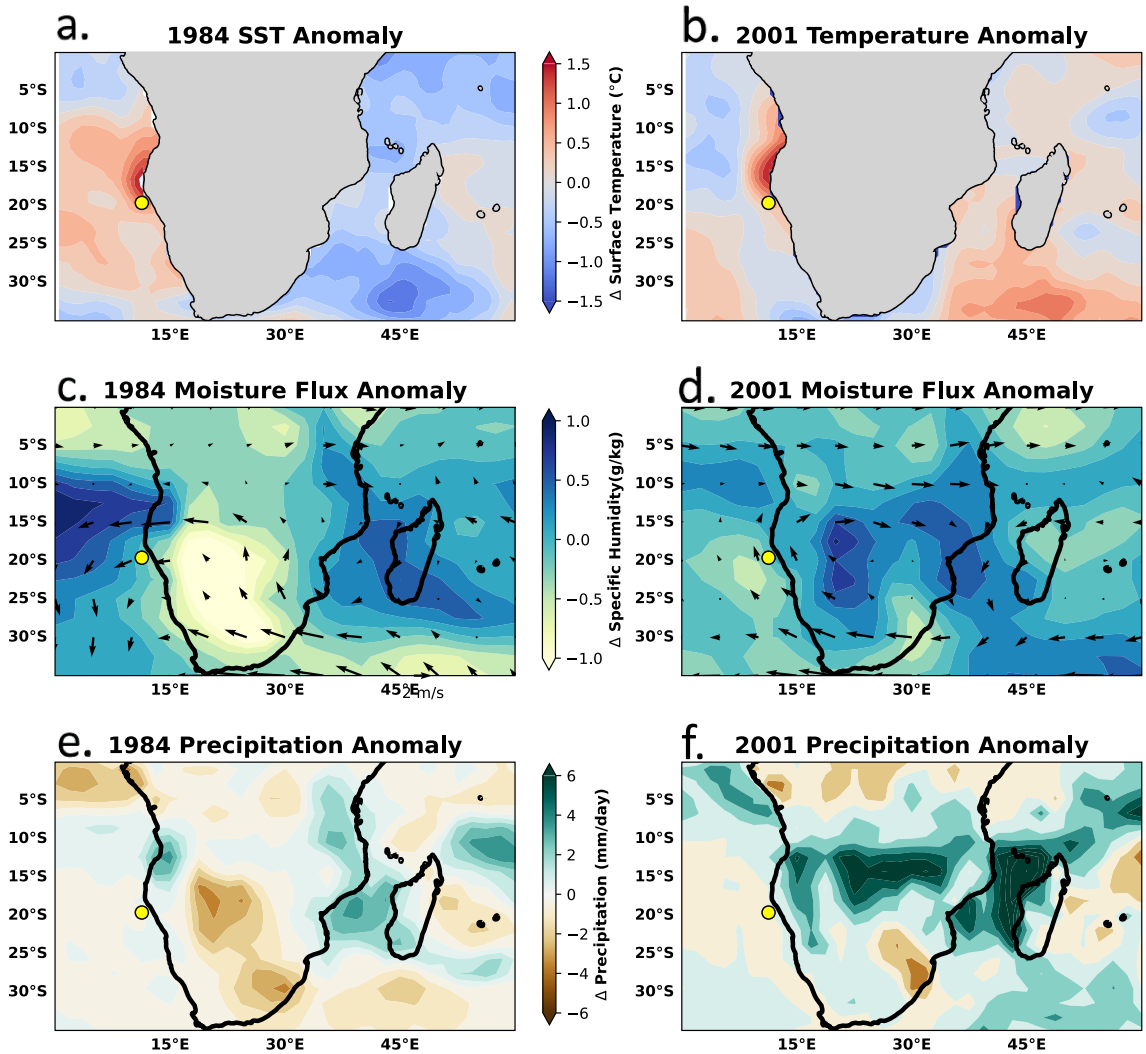

Figure 2. Top: Mean JFM sea surface temperature anomalies for the 1984 (a) and 2001 (b) Benguela Niño events, taken from NCEP-NCAR reanalysis data. Middle: Mean JFM integrated moisture from surface to 300 hPa flux anomalies for 1984 (c) and 2001 (d) events in kg/kg.m/s. Bottom: Mean JFM precipitation anomalies for 1984 (e) and 2001 (f) in mm/day. The yellow circles mark the location of ODP 1081.

temperature anomalies of 1.0–1.5° in the BUS, but negative temperature anomalies (−1 to −1.5°) in the Indian Ocean (Figure 2). In contrast, the 2001 Benguela Niño is associated with a similar magnitude of BUS warming, but positive temperature anomalies (0.25–0.8°) in the Indian Ocean. The contrasting patterns of low level winds, moisture flux, and precipitation highlight the modulating effect of Indian Ocean SSTs.

The 1984 Benguela Niño features a negative SST over the Indian Ocean (Figure 2) and an enhanced Botswana high pressure system (Rouault et al., 2003). This limited moisture availability and resulted in only a localized increase in precipitation over Namibia at 10°S (Hansingo & Reason, 2009; Rouault et al., 2003). In contrast, the 2001 Benguela Niño, which co-occurred with anomalously warm Indian Ocean SSTs, features a weaker Botswana high pressure system, enhanced moisture convergence, and larger precipitation increases over the continent (Rouault et al., 2003). These results cohere with idealized experiments by Hansingo and Reason (2009), which tested the sensitivity of the regional atmosphere to the location of Benguela and Indian Ocean SST anomalies. SSTs anomalies in the southwest Indian Ocean were shown to augment or oppose Benguela Niño impacts, though an Indian Ocean SST anomaly is not required for Benguela Niños to produce anomalous rainfall (Hansingo & Reason, 2009).

Drawing on this observational analog, we suggest that the Plio-Pleistocene depletion trend in the ODP 1081 δD_p record reflects changes in hydroclimate related to BUS temperatures. However, sub-million year scale intervals of shifts to more depleted values (e.g., between 3.5 and 2.9 Ma and between 1.5 and 1 Ma) may reflect intervals of

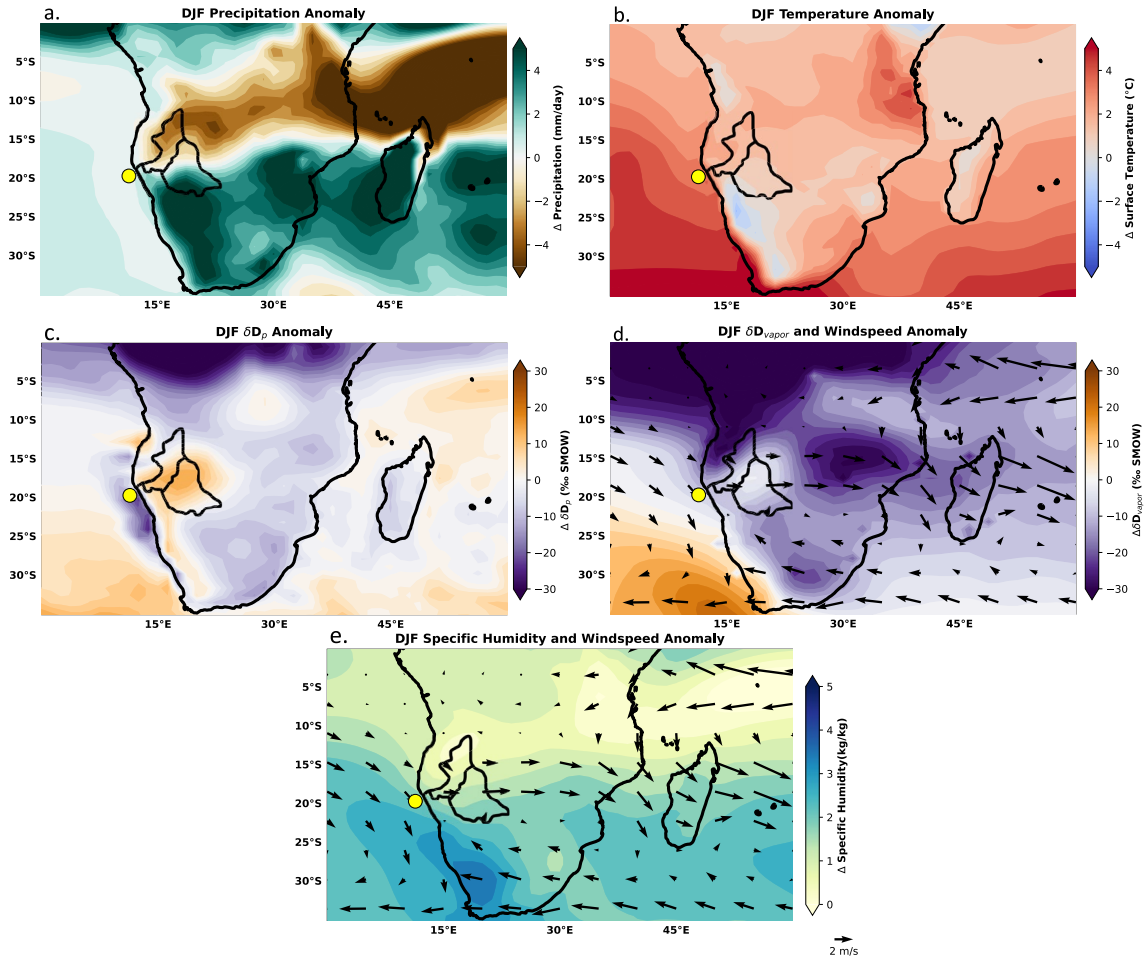

Figure 3. Pliocene anomalies (Pliocene - PI) simulated in iCAM5 for DJF. (a) Simulated precipitation anomalies. (b) Simulated surface temperature and proxy reconstructed sea surface temperature (SST) anomalies calculated from alkenone SST records from ODP 1081, 1082, and 1084. (c) Simulated δD_p and proxy reconstructed δD_p anomalies calculated from leaf wax records for ODP 1081 and 1085, and measurements of nearby coretop samples. (d) Simulated wind speed anomalies (arrows) and δD_{vapor} anomalies (vertically integrated to 500 hPa). From north to south, the black outlines in each panel show the Kunene and Cuvelai Basins. The yellow circles mark the location of ODP 1081.

cooler Indian Ocean SST. The interval from 3.5 to 2.9 Ma may have resembled the 1984 event, with cooler Indian Ocean SSTs contributing to muted precipitation anomalies and relatively depleted δD_p values. The similarity between modern Benguela Niño s and mid-Pliocene conditions has been noted by Rosell-Melé et al. (2014), however the physical mechanisms driving this pattern in the Pliocene have not yet been explored through the lens of climate models. It is possible that BUS and Indian Ocean SSTs interact in complex ways to modulate hydroclimate over Namibia, and fully evaluating this hypothesis would benefit from more Plio-Pleistocene records of southwestern Indian Ocean SSTs.

3.4. Southwest African Hydroclimate in iCAM5

When forced with Pliocene-like SSTs, iCAM5 produces a zonal shift in precipitation. A negative precipitation anomaly stretches across the continent and Indian Ocean along the ∼10–20° latitude band, with wetter conditions to the south. Modeled δD_p is depleted relative to the preindustrial over much of SWA (Figure 3c). However, a strip of land along the Namib coast, including the Cuvelai basin, has enriched precipitation, consistent with the signal observed in our proxy records. The spatial pattern of δD_{vapor} over land is similar to δD_p (Figure 3d). This zone of enriched precipitation could be explained by northwesterly wind anomalies off the coast of SWA that transport anomalously enriched vapor from the tropical Atlantic (Figures 3d and 3e), or may be related to localized changes in surface temperature (Figure 3b).

The hydroclimate changes produced by iCAM5 are broadly consistent with what we expect during a Benguela Niño event (e.g., 2001) featuring warming in both the BUS and southwest Indian Ocean. However, while during

the 2001 Benguela Niño positive precipitation anomalies occurred over the 15 to 20°S latitude band, the model simulation shows increased precipitation occurs south of 20°S. Additionally, where the 2001 event featured a weakened Botswana High, iCAM5 simulates a slightly enhanced Botswana High (Figure S6 in Supporting Information S1). The local zone of enriched vapor simulated over the Cuvelai basin is broadly consistent with the signal at ODP 1081. However, the simulated zonal band of drying at 10–20°S is inconsistent with available paleobotanical evidence (Dupont, 2006; Dupont et al., 2005).

3.5. Comparison to PlioMIP2

We next shift our focus to the PlioMIP2 ensemble, which features fully-coupled model simulations of the mid-Piacenzian warm period (MPWP), between 3.264 and 3.025 Ma. Over the BUS, PlioMIP2 models show widely varying SST changes; all but four models underestimate warming seen in the ODP 1081 SST record (Figure S7 in Supporting Information S1).

Nine of 13 PlioMIP2 models simulate a drier MPWP, at odds with our interpretation of the δD_p record at ODP 1081. Only four models (CESM 1.2, NorESM, IPSL-CM6, and EC-Earth 3.3) simulate a precipitation response over the ODP 1081 source area that is consistent with more mesic conditions inferred from our record and previous paleobotanical proxy data from SWA (Dupont et al., 2005). Figure 4 contrasts the average DJF precipitation

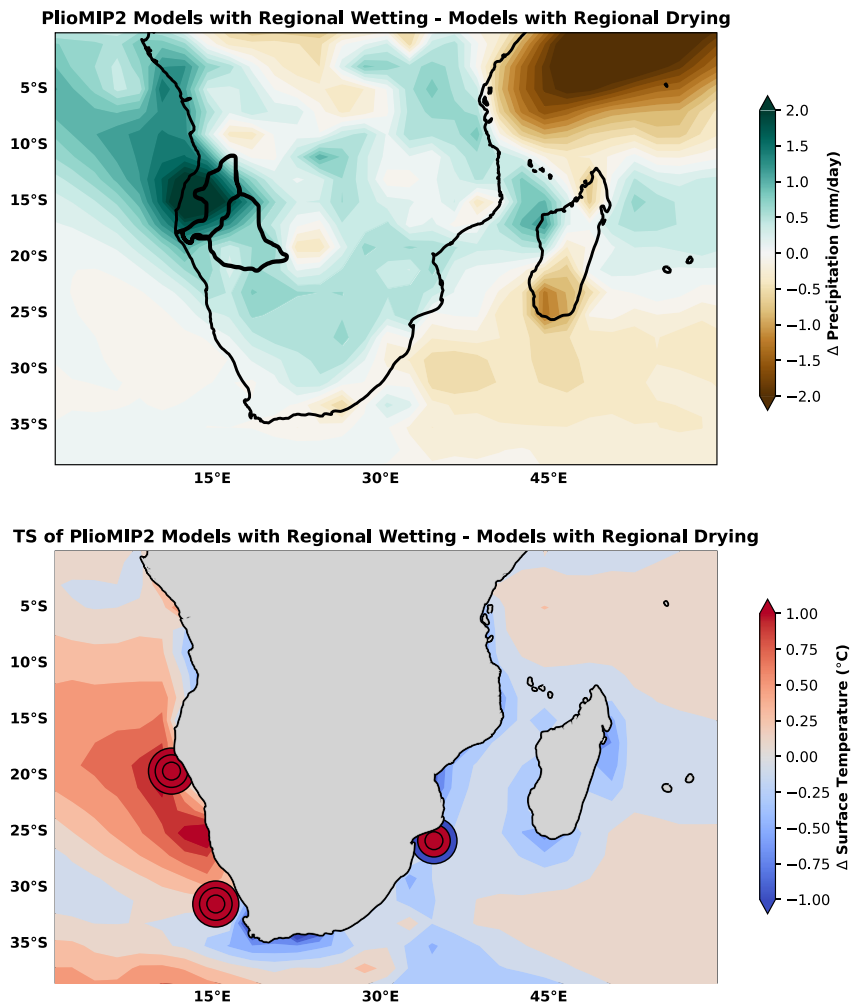

Figure 4. (a) DJF mean precipitation anomalies between PlioMIP2 models with positive mid-Pliocene - PI precipitation anomalies (i.e., wetting) over the ODP 1081 source area and models with negative mid-Pliocene - PI precipitation anomalies (i.e., drying) over the ODP 1081 source area. (b) Surface temperature (TS) anomalies for these same models. Sea surface temperature anomalies were calculated from proxy records and modern observations for ODP 1081, 1087 and IODP U1478. Layered circles show the 5% (outer ring), 50% (median, middle ring), and 95% confidence intervals (inner circle).

and surface temperature response of the four wet models with the average of all PlioMIP2 models, highlighting the increased precipitation over the ODP 1081 source area. Compared to the full model ensemble, CESM 1.2, NorESM, IPSL-CM6, and EC-Earth 3.3 simulate warmer SSTs in the BUS and cooler SSTs in the western Indian Ocean than the models that show drying in the ODP 1081 source region. This suggests that the temperature gradient between the BUS and western Indian Ocean determines the location and strength of the precipitation anomaly, and is an important source of intermodel disagreement. Prior analyses by Brierley et al. (2009) and Corvec and Fletcher (2017) similarly argue that warmer subtropical SSTs, especially in coastal upwelling systems, result in wetter conditions. Further interrogation of dynamical and thermodynamic components of PlioMIP2 can shed light on whether a Benguela Niño-like mechanism is at work in those models.

4. Conclusions

A new Plio-Pleistocene δD_p record from ODP 1081 shows a strong relationship with long-term cooling in the BUS, but with low frequency variability that most likely reflects hydroclimate modulation by Indian Ocean temperatures. The scarcity of Pliocene Indian Ocean SST records limits our ability to investigate this driver from a proxy perspective, and higher-resolution studies are needed to analyze orbital-scale variability.

Nevertheless, using observational data, we identified a mechanism by which Indian Ocean SSTs modulate the strength of convection over southern Africa, similar to what occurs during Benguela Niños in the present day. Our results agree with previous work demonstrating that warming of upwelling zones drove reorganizations of subtropical hydroclimate (Bhattacharya et al., 2022; Brierley et al., 2009; Corvec & Fletcher, 2017). When forced with Pliocene SSTs, iCAM5 produces a local isotopic enrichment over the Cuvelai basin, but simulates drying over the ODP 1081 leaf wax source area. This may be related to large-scale SST gradient changes in the model, and can be explored with further idealized simulations. This comparison highlights the utility of paleohydrological proxies for benchmarking model performance.

Finally, our results offer insights into PlioMIP2 model performance. Only four of 13 models simulated the correct sign of precipitation change, as implied by proxy evidence. Model analysis shows that three models performed better than the ensemble mean by capturing a reduced zonal temperature gradient between the Indian and South Atlantic oceans. While other factors like insolation and direct CO_2 effects may influence hydroclimate, this multi-model analysis shows that accurately capturing regional SST patterns appears to be key to simulating past hydrological variability. Understanding why certain models produce differing Atlantic-Indian ocean SST patterns could reveal the model configurations that will produce reliable predictions of future regional hydroclimate change in southwestern Africa.

Conflict of Interest

T. Bhattacharya is an associate editor for Geophysical Research Letters, but was recused from the review process to avoid conflict of interest. The authors declare no other conflicts of interest.

Data Availability Statement

Newly generated data sets from ODP 1081 are available on the NOAA/NCEI Paleoclimatology Database (https://www.ncei.noaa.gov/access/paleo-search/study/37258) (Rubbelke et al., 2023). Model simulations used in this paper are previously published in Knapp et al. (2022b) and available at https://doi.org/10.5281/zenodo.6953979 (Knapp et al., 2022a). The PlioMIP2 simulations analyzed in this study that are part of the Climate Model Intercomparison Project 6 have been deposited to the Earth System Grid Federation. Processed precipitation and surface temperature data is part of Feng et al. (2022a), and can be accessed at:https://doi.org/10.5281/zenodo.5706370.

Acknowledgments
TB and CR acknowledge funding support from NSF Grants Paleo Perspectives on Climate Change (P2C2) OCE-1903148 and OCE-2103015. RF acknowledges funding support from OCE-1903650 and OCE-2103055. Measurements were made possible with support from NSF MRI Grant EAR-2018078 to TB. We thank the members of the Paleoclimate Dynamics Lab and PaleoX groups at Syracuse University, especially Jillian Aluisio and Stephanie Bullinger. Chris Maupin at Texas A&M and Andrew Cooper (Thermo) provided crucial remote instrumentation support.

References

Aggarwal, P. K., Romatschke, U., Araguas-Araguas, L., Belachew, D., Longstaae, F. J., Berg, P., et al. (2016). Proportions of convective and stratiform precipitation revealed in water isotope ratios. *Nature Geoscience*, *9*(8), 624–629. https://doi.org/10.1038/NGEO2739

Arnault, J., Niezgoda, K., Jung, G., Hahn, A., Zabel, M., Schefuß, E., & Kunstmann, H. (2022). Disentangling the contribution of moisture source change to isotopic proxy signatures: Deuterium tracing with WRF-Hydro-iso-tag and application to Southern African Holocene sediment archives. *Journal of Climate*, *35*(22), 3855–3879. https://doi.org/10.1175/jcli-d-22-0041.1

Astropy Collaboration, Price-Whelan, A. M., Lim, P. L., Earl, N., Starkman, N., Bradley, L., et al. (2022). The Astropy Project: Sustaining and growing a community-oriented open-source project and the latest major release (v5.0) of the core package [Software]. The Astrophysical Journal, *935*(2), 167. https://doi.org/10.3847/1538-4357/ac7c74

Bachèlery, M.-L., Illig, S., & Rouault, M. (2020). Interannual coastal trapped waves in the Angola-Benguela upwelling system and Benguela Niño and Niña events. *Journal of Marine Systems*, *203*, 103262. https://doi.org/10.1016/j.jmarsys.2019.103262

Baxter, A., Verschuren, D., Peterse, F., Miralles, D., Martin-Jones, C., Maitituerdi, A., et al. (2023). Reversed Holocene temperature–moisture relationship in the Horn of Africa. *Nature*, *620*(7973), 336–343. https://doi.org/10.1038/s41586-023-06272-5

Belz, L., Schüller, I., Wehrmann, A., Köster, J., & Wilkes, H. (2020). The leaf wax biomarker record of a Namibian salt pan reveals enhanced summer rainfall during the Last Glacial-Interglacial Transition. *Palaeogeography, Palaeoclimatology, Palaeoecology*, *543*, 109561. https://doi.org/10.1016/j.palaeo.2019.109561

Bhattacharya, T., Feng, R., Tierney, J. E., Rubbelke, C., Burls, N., Knapp, S., & Fu, M. (2022). Expansion and intensification of the North American Monsoon during the Pliocene. *AGU Advances*, *3*(6), e2022AV000757. https://doi.org/10.1029/2022AV000757

Brierley, C. M., Fedorov, A. V., Liu, Z., Herbert, T. D., Lawrence, K. T., & Lariviere, J. (2009). Greatly expanded tropical warm pool and weakened Hadley circulation in the early Pliocene. *Science*, *323*, 1714–1719. https://doi.org/10.1126/science.1167625

Burke, K. D., Williams, J. W., Chandler, M. A., Haywood, A. M., Lunt, D. J., & Otto-Bliesner, B. L. (2018). Pliocene and Eocene provide best analogs for near-future climates. *Proceedings of the National Academy of Sciences*, *115*(52), 13288–13293. https://doi.org/10.5061/dryad.0j18k00

Burls, N. J., Blamey, R. C., Cash, B. A., Swenson, E. T., al Fahad, A., Bopape, M. J. M., et al. (2019). The Cape Town "day zero" drought and Hadley cell expansion. *npj Climate and Atmospheric Science*, *2*(1), 27. https://doi.org/10.1038/s41612-019-0084-6

Burls, N. J., & Fedorov, A. V. (2014). Simulating Pliocene warmth and a permanent El Niño-like state: The role of cloud albedo. *Paleoceanography*, *29*(10), 893–910. https://doi.org/10.1002/2014PA002644

Burls, N. J., & Fedorov, A. V. (2017). Wetter subtropics in a warmer world: Contrasting past and future hydrological cycles. *Proceedings of the National Academy of Sciences of the United States of America*, *114*(49), 12888–12893. https://doi.org/10.1073/pnas.1703421114

Byrne, M. P., & O'Gorman, P. A. (2015). The response of precipitation minus evapotranspiration to climate warming: Why the "wet-get-wetter, dry-get-drier" scaling does not hold over land. *Journal of Climate*, *28*(20), 8078–8092. https://doi.org/10.1175/JCLI-D-15-0369.1

Cohen, A. S., Du, A., Rowan, J., Yost, C. L., Billingsley, A. L., Campisano, C. J., & Brown, E. T. (2022). Plio-Pleistocene environmental variability in Africa and its implications for mammalian evolution. *Proceedings of the National Academy of Sciences*, *119*(16), e2107393119. https://doi.org/10.1073/pnas.2107393119/-/DCSupplemental.Published

Collins, J. A., Schefuß, E., Mulitza, S., Prange, M., Werner, M., Tharammal, T., et al. (2013). Estimating the hydrogen isotopic composition of past precipitation using leaf-waxes from western Africa. *Quaternary Science Reviews*, *65*, 88–101. https://doi.org/10.1016/j.quascirev.2013.01.007

Corvec, S., & Fletcher, C. G. (2017). Changes to the tropical circulation in the mid-Pliocene and their implications for future climate. *Climate of the Past*, *13*(2), 135–147. https://doi.org/10.5194/cp-13-135-2017

de la Vega, E., Chalk, T. B., Wilson, P. A., Bysani, R. P., & Foster, G. L. (2020). Atmospheric CO_2 during the Mid-Piacenzian Warm Period and the M2 glaciation. *Scientific Reports*, *10*(1). 11002. https://doi.org/10.1038/s41598-020-67154-8

Diefendorf, A. F., & Freimuth, E. J. (2017). Extracting the most from terrestrial plant-derived *n*-alkyl lipids and their carbon isotopes from the sedimentary record: A review. *Organic Geochemistry*, *103*, 1–21. https://doi.org/10.1016/j.orggeochem.2016.10.016

Dupont, L. M. (2006). Late Pliocene vegetation and climate in Namibia (southern Africa) derived from palynology of ODP Site 1082. *Geochemistry, Geophysics, Geosystems*, *7*(5), Q05007. https://doi.org/10.1029/2005GC001208

Dupont, L. M., Donner, B., Pé, E. M., & Wefer, G. (2005). Linking desert evolution and coastal upwelling: Pliocene climate change in Namibia. *Geology*, *33*(6), 461–464. https://doi.org/10.1130/G21401.1

Dupont, L. M., Rommerskirchen, F., Mollenhauer, G., & Schefuß, E. (2013). Miocene to Pliocene changes in South African hydrology and vegetation in relation to the expansion of C4 plants. *Earth and Planetary Science Letters*, *375*, 408–417. https://doi.org/10.1016/j.epsl.2013.06.005

Dupont, L. M., & Wyputta, U. (2003). Reconstructing pathways of aeolian pollen transport to the marine sediments along the coastline of SW Africa. *Quaternary Science Reviews*, *22*(2–4), 157–174. https://doi.org/10.1016/s0277-3791(02)00032-x

Eckardt, F. D., Soderberg, K., Coop, L. J., Muller, A. A., Vickery, K. J., Grandin, R. D., et al. (2013). The nature of moisture at Gobabeb, in the central Namib Desert. *Journal of Arid Environments*, *93*, 7–19. https://doi.org/10.1016/j.jaridenv.2012.01.011

Etourneau, J., Martinez, P., Blanz, T., & Schneider, R. (2009). Pliocene-Pleistocene variability of upwelling activity, productivity, and nutrient cycling in the Benguela region. *Geology*, *37*(10), 871–874. https://doi.org/10.1130/G25733A.1

Feakins, S. J. (2013). Pollen-corrected leaf wax D/H reconstructions of northeast African hydrological changes during the late Miocene. *Palaeogeography, Palaeoclimatology, Palaeoecology*, *374*, 62–71. https://doi.org/10.1016/j.palaeo.2013.01.004

Feakins, S. J., Peter, B., & Eglinton, T. I. (2005). Biomarker records of late Neogene changes in northeast African vegetation. *Biomarker records of late Neogene changes in northeast African vegetation*, *33*(12), 977–980. https://doi.org/10.1130/G21814.1

Feakins, S. J., & Sessions, A. L. (2010). Controls on the D/H ratios of plant leaf waxes in an arid ecosystem. *Geochimica et Cosmochimica Acta*, *74*(7), 2128–2141. https://doi.org/10.1016/j.gca.2010.01.016

Feng, R., Bhattacharya, T., Otto-Bliesner, B. L., Brady, E. C., Haywood, A. M., Tindall, J. C., et al. (2022a). Data for past terrestrial hydroclimate sensitivity controlled by Earth system feedbacks [Dataset]. Zenodo. https://doi.org/10.5281/zenodo.5706370

Feng, R., Bhattacharya, T., Otto-Bliesner, B. L., Brady, E. C., Haywood, A. M., Tindall, J. C., et al. (2022b). Past terrestrial hydroclimate sensitivity controlled by Earth system feedbacks. *Nature Communications*, *13*, 1306. https://doi.org/10.1038/s41467-022-28814-7

Fleming, L. E., & Tierney, J. E. (2016). An automated method for the determination of the TEX86 and U37K′ paleotemperature indices. *Organic Geochemistry*, *92*, 84–91. https://doi.org/10.1016/j.orggeochem.2015.12.011

Florenchie, P., Lutjeharms, J. R., Reason, C. J. C., Masson, S., & Rouault, M. (2003). The source of Benguela Niños in the South Atlantic Ocean. *Geophysical Research Letters*, *30*(10), 10–13. https://doi.org/10.1029/2003gl017172

Freimuth, E. J., Diefendorf, A. F., & Lowell, T. V. (2017). Hydrogen isotopes of *n*-alkanes and *n*-alkanoic acids as tracers of precipitation in a temperate forest and implications for paleorecords. *Geochimica et Cosmochimica Acta*, *206*, 166–183. https://doi.org/10.1016/j.gca.2017.02.027

Fu, M., Cane, M. A., Molnar, P., & Tziperman, E. (2021). Wetter subtropics lead to reduced Pliocene coastal upwelling. *Paleoceanography and Paleoclimatology*, *36*(10), 1–22. https://doi.org/10.1029/2021PA004243

Gao, L., Edwards, E. J., Zeng, Y., & Huang, Y. (2014). Major evolutionary trends in hydrogen isotope fractionation of vascular plant leaf waxes. *PLoS One*, *9*(11), 112610. https://doi.org/10.1371/journal.pone.0112610

Garcin, Y., Schefuß, E., Schwab, V. F., Garreta, V., Gleixner, G., Vincens, A., et al. (2014). Reconstructing C3 and C4 vegetation cover using *n*-alkane carbon isotope ratios in recent lake sediments from Cameroon, western central Africa. *Geochimica et Cosmochimica Acta*, *142*, 482–500. https://doi.org/10.1016/j.gca.2014.07.004

Garelick, S., Russell, J. M., Dee, S., Verschuren, D., & Olago, D. O. (2021). Atmospheric controls on precipitation isotopes and hydroclimate in high-elevation regions in Eastern Africa since the Last Glacial Maximum. *Earth and Planetary Science Letters*, *567*, 116984. https://doi.org/10.1016/j.epsl.2021.116984

Good, S. P., Noone, D., Kurita, N., Benetti, M., & Bowen, G. J. (2015). D/H isotope ratios in the global hydrologic cycle. *Geophysical Research Letters*, *42*(12), 5042–5050. https://doi.org/10.1002/2015gl064117

Griepentrog, M., De Wispelaere, L., Bauters, M., Bodé, S., Hemp, A., Verschuren, D., & Boeckx, P. (2019). Influence of plant growth form, habitat and season on leaf-wax *n*-alkane hydrogen-isotopic signatures in equatorial East Africa. *Geochimica et Cosmochimica Acta*, *263*, 122–139. https://doi.org/10.1016/j.gca.2019.08.004

Hansingo, K., & Reason, C. J. C. (2009). Modelling the atmospheric response over southern Africa to SST forcing in the southeast tropical Atlantic and southwest subtropical Indian Oceans. *International Journal of Climatology*, *29*(7), 1001–1012. https://doi.org/10.1002/joc.1919

Haywood, A. M., Tindall, J. C., Dowsett, H. J., Dolan, A. M., Foley, K. M., Hunter, J., et al. (2020). A return to large-scale features of Pliocene climate: The Pliocene Model Intercomparison Project Phase 2. *Climate of the Past*, 1–40. https://doi.org/10.5194/cp-2019-145

Held, I. M., & Soden, B. J. (2006). Robust responses of the hydrological cycle to global warming. *Journal of Climate*, *19*(21), 5686–5699. https://doi.org/10.1175/jcli3990.1

Hemingway, J. D., Rothman, D. H., Grant, K. E., Rosengard, S. Z., Eglinton, T. I., Derry, L. A., & Galy, V. V. (2019). Mineral protection regulates long-term global preservation of natural organic carbon. *Nature*, *570*(7760), 228–231. https://doi.org/10.1038/s41586-019-1280-6

Herrmann, N., Boom, A., Carr, A. S., Chase, B. M., West, A. G., Zabel, M., & Schefuß, E. (2017). Hydrogen isotope fractionation of leaf wax *n*-alkanes in southern African soils. *Organic Geochemistry*, *109*, 1–13. https://doi.org/10.1016/j.orggeochem.2017.03.008

Hipondoka, M. H. (2005). *The development and evolution of Etosha Pan, Namibia* (Unpublished doctoral dissertation). Universität Würzburg.

Hoetzel, S., Dupont, L., Schefuß, E., Rommerskirchen, F., & Wefer, G. (2013). The role of fire in Miocene to Pliocene C4 grassland and ecosystem evolution. *Nature Geoscience*, *6*(12), 1027–1030. https://doi.org/10.1038/ngeo1984

Hoetzel, S., Dupont, L. M., & Wefer, G. (2015). Miocene-Pliocene vegetation change in south-western Africa (ODP Site 1081, offshore Namibia). *Palaeogeography, Palaeoclimatology, Palaeoecology*, *423*, 102–108. https://doi.org/10.1016/j.palaeo.2015.02.002

Huang, N. E., Shen, Z., Long, S. R., Wu, M. C., Shih, H. H., Zheng, Q., et al. (1998). The empirical mode decomposition and the Hilbert spectrum for nonlinear and non-stationary time series analysis. *Proceedings of the Royal Society of London. Series A: Mathematical, Physical and Engineering Sciences*, *454*(1971), 903–995. https://doi.org/10.1098/rspa.1998.0193

Hurrell, J. W., Hack, J. J., Shea, D., Caron, J. M., & Rosinski, J. (2008). A new sea surface temperature and sea ice boundary dataset for the Community Atmosphere Model. *Journal of Climate*, *21*(19), 5145–5153. https://doi.org/10.1175/2008jcli2292.1

Hutchings, L., van der Lingen, C. D., Shannon, L. J., Crawford, R. J., Verheye, H. M., Bartholomae, C. H., et al. (2009). The Benguela Current: An ecosystem of four components. *Progress in Oceanography*, *83*(1–4), 15–32. https://doi.org/10.1016/j.pocean.2009.07.046

Inglis, G. N., Bhattacharya, T., Hemingway, J. D., Hollingsworth, E. H., Feakins, S. J., & Tierney, J. E. (2022). Biomarker approaches for reconstructing terrestrial environmental change. *Annual Review of Earth and Planetary Sciences*, *50*(1), 369–394. https://doi.org/10.1146/annurev-earth-032320-095943

IPCC. (2014). Climate Change 2014: Synthesis Report. Contribution of Working Groups I, II, and III to the Fifth Assessment Report of the Intergovernmental Panel on Climate Change (Technical Report). https://doi.org/10.1016/S0022-0248(00)00575-3

Jeng, W. L. (2006). Higher plant *n*-alkane average chain length as an indicator of petrogenic hydrocarbon contamination in marine sediments. *Marine Chemistry*, *102*(3–4), 242–251. https://doi.org/10.1016/j.marchem.2006.05.001

Kaseke, K. F., Wang, L., Wanke, H., Turewicz, V., & Koeniger, P. (2016). An analysis of precipitation isotope distributions across Namibia using historical data. *PLoS One*, *11*(5), 1–19. https://doi.org/10.1371/journal.pone.0154598

Knapp, S., Burls, N., Dee, S., Feng, R., Feakins, S. J., & Bhattacharya, T. (2022a). Data for article "A Pliocene precipitation isotope proxy-model comparison assessing the hydrological fingerprints of sea surface temperature gradients" [Dataset]. Zenodo. https://doi.org/10.5281/zenodo.6953979

Knapp, S., Burls, N. J., Dee, S., Feng, R., Feakins, S. J., & Bhattacharya, T. (2022b). A Pliocene precipitation isotope proxy-model comparison assessing the hydrological fingerprints of sea surface temperature gradients. *Paleoceanography and Paleoclimatology*, *37*(12), e2021PA004401. https://doi.org/10.1029/2021pa004401

Konecky, B. L., Russell, J. M., Johnson, T. C., Brown, E. T., Berke, M. A., Werne, J. P., & Huang, Y. (2011). Atmospheric circulation patterns during late Pleistocene climate changes at Lake Malawi, Africa. *Earth and Planetary Science Letters*, *312*(3–4), 318–326. https://doi.org/10.1016/j.epsl.2011.10.020

Kuechler, R. R., Dupont, L. M., & Schefuß, E. (2018). Hybrid insolation forcing of Pliocene monsoon dynamics in West Africa. *Climate of the Past*, *14*(1), 73–84. https://doi.org/10.5194/cp-14-73-2018

Kusangaya, S., Warburton, M. L., Archer, E., Garderen, V., & Jewitt, G. P. W. (2014). Impacts of climate change on water resources in southern Africa: A review. *Physics and Chemistry of the Earth*, *67–69*, 47–54. https://doi.org/10.1016/j.pce.2013.09.014

Li, X., Wang, M., Zhang, Y., Lei, L., & Hou, J. (2017). Holocene climatic and environmental change on the western Tibetan Plateau revealed by glycerol dialkyl glycerol tetraethers and leaf wax deuterium-to-hydrogen ratios at Aweng Co. *Quaternary Research*, *87*(3), 455–467. https://doi.org/10.1017/qua.2017.9

Lisiecki, L. E., & Raymo, M. E. (2005). A Pliocene-Pleistocene stack of 57 globally distributed benthic $\delta^{18}O$ records. *Paleoceanography*, *20*, 1–17. https://doi.org/10.1029/2004PA001071

Liu, H., Wang, S., Wang, H., Cao, Y., Hu, J., & Liu, W. (2023). Apparent fractionation of hydrogen isotope from precipitation to leaf wax *n*-alkanes from natural environments and manipulation experiments. *Science of the Total Environment*, *877*, 162970. https://doi.org/10.1016/j.scitotenv.2023.162970

Lupien, R. L., Russell, J. M., Pearson, E. J., Castañeda, I. S., Asrat, A., Foerster, V., et al. (2022). Orbital controls on eastern African hydroclimate in the Pleistocene. *Scientific Reports*, *12*(1), 3170. https://doi.org/10.1038/s41598-022-06826-z

Lupien, R. L., Russell, J. M., Subramanian, A., Kinyanjui, R., Beverly, E. J., Uno, K. T., et al. (2021). Eastern African environmental variation and its role in the evolution and cultural change of Homo over the last 1 million years. *Journal of Human Evolution*, *157*, 103028. https://doi.org/10.1016/j.jhevol.2021.103028

Marlow, J. R., Lange, C. B., Wefer, G., & Rosell-Melé, A. (2000). Upwelling intensification as part of the Pliocene-Pleistocene climate transition (Technical Report). https://doi.org/10.1126/science.290.5500.2288

Maupin, C. R., Roark, E. B., Thirumalai, K., Shen, C.-C., Schumacher, C., Kampen-Lewis, V., et al. (2021). Abrupt Southern Great Plains thunderstorm shifts linked to glacial climate variability. *Nature Geoscience*, *14*(6), 396–401. https://doi.org/10.1038/s41561-021-00729-w

Muller, A., Reason, C. J. C., & Fauchereau, N. (2007). Extreme rainfall in the Namib Desert during late summer 2006 and influences of regional ocean variability. *International Journal of Climatology*, *28*(8), 1061–1070. https://doi.org/10.1002/joc

Nicholson, S. E. (2010). A low-level jet along the Benguela coast, an integral part of the Benguela current ecosystem. *Climatic Change*, *99*(3), 613–624. https://doi.org/10.1007/s10584-009-9678-z

Nusbaumer, J., Wong, T. E., Bardeen, C., & Noone, D. (2017). Evaluating hydrological processes in the Community Atmosphere Model Version 5 (CAM5) using stable isotope ratios of water. *Journal of Advances in Modeling Earth Systems*, *9*(2), 949–977. https://doi.org/10.1002/2016MS000842.Key

Ogega, O. M., Gyampoh, B. A., & Mistry, M. N. (2020). Intraseasonal precipitation variability over West Africa under 1.5°C and 2.0°C global warming scenarios: Results from CORDEX RCMs. *Climate*, *8*(12), 143. https://doi.org/10.3390/cli8120143

Petrick, B., Mcclymont, E. L., Felder, S., Rueda, G., Leng, M. J., & Rosell-Melé, A. (2015). Late Pliocene upwelling in the Southern Benguela region. *Palaeogeography, Palaeoclimatology, Palaeoecology*, *429*, 62–71. https://doi.org/10.1016/j.palaeo.2015.03.042

Pontes, G. M., Wainer, I., Taschetto, A. S., Sen Gupta, A., Abe-Ouchi, A., Brady, E. C., et al. (2020). Drier tropical and subtropical Southern Hemisphere in the mid-Pliocene warm period. *Scientific Reports*, *10*(1), 1–11. https://doi.org/10.1038/s41598-020-68884-5

Quinn, A. J., Lopes-dos Santos, V., Dupret, D., Nobre, A. C., & Woolrich, M. W. (2021). EMD: Empirical mode decomposition and Hilbert-Huang spectral analyses in Python. *Journal of Open Source Software*, *6*(59), 2977. https://doi.org/10.21105/joss.02977

Rae, J. W. B., Zhang, Y. G., Liu, X., Foster, G. L., Stoll, H. M., & Whiteford, R. D. M. (2021). Atmospheric CO_2 over the past 66 million years from marine archives. *The Annual Review of Earth and Planetary Sciences is online at earth.annualreviews.org*, *49*(1), 609–650. https://doi.org/10.1146/annurev-earth-082420

Reason, C. J. C. (2001). Subtropical Indian Ocean SST dipole events and southern African rainfall. *Geophysical Research Letters*, *28*(11), 2225–2227. https://doi.org/10.1029/2000gl012735

Reason, C. J. C., Florenchie, P., Rouault, M., & Veitch, J. (2006). Influences of large scale climate modes and Agulhas system variability on the BCLME region. *Large Marine Ecosystems*, *14*, 223–238.

Reason, C. J. C., Landman, W., & Tennant, W. (2006). Seasonal to decadal prediction of southern African climate and its links with variability of the Atlantic Ocean. *Bulletin of the American Meteorological Society*, *87*(7), 941–956. https://doi.org/10.1175/bams-87-7-941

Rosell-Melé, A., Martínez-Garcia, A., & Mcclymont, E. L. (2014). Persistent warmth across the Benguela upwelling system during the Pliocene epoch. *Earth and Planetary Science Letters*, *386*, 10–20. https://doi.org/10.1016/j.epsl.2013.10.041

Rouault, M., Florenchie, P., Fauchereau, N., & Reason, C. J. C. (2003). South East tropical Atlantic warm events and southern African rainfall. *Geophysical Research Letters*, *30*(5), 8009. https://doi.org/10.1029/2002GL014840

Rouault, M., Illig, S., Bartholomae, C., Reason, C. J. C., & Bentamy, A. (2007). Propagation and origin of warm anomalies in the Angola Benguela upwelling system in 2001. *Journal of Marine Systems*, *68*(3–4), 473–488. https://doi.org/10.1016/j.jmarsys.2006.11.010

Rubbelke, C., Bhattacharya, T., Feng, R., Burls, N., Knapp, S., & McClymont, E. (2023). Plio-Pleistocene Southwest African Hydroclimate modulated by Benguela and Indian Ocean temperatures [Dataset]. National Centers for Environmental Information. Retrieved from https://www.ncei.noaa.gov/access/paleo-search/study/37258

Sachse, D., Billault, I., Bowen, G. J., Chikaraishi, Y., Dawson, T. E., Feakins, S. J., et al. (2012). Molecular paleohydrology: Interpreting the hydrogen-isotopic composition of lipid biomarkers from photosynthesizing organisms. *Annual Review of Earth and Planetary Sciences*, *40*(1), 221–249. https://doi.org/10.1146/annurev-earth-042711-105535

Sachse, D., Radke, J., & Gleixner, G. (2004). Hydrogen isotope ratios of recent lacustrine sedimentary *n*-alkanes record modern climate variability. *Geochimica et Cosmochimica Acta*, *68*(23), 4877–4889. https://doi.org/10.1016/j.gca.2004.06.004

Seager, R., Naik, N., & Vecchi, G. A. (2010). Thermodynamic and dynamic mechanisms for large-scale changes in the hydrological cycle in response to global warming. *Journal of Climate*, *23*(17), 4651–4668. https://doi.org/10.1175/2010JCLI3655.1

Seo, K. H., Frierson, D. M., & Son, J. H. (2014). A mechanism for future changes in Hadley circulation strength in CMIP5 climate change simulations. *Geophysical Research Letters*, *41*(14), 5251–5258. https://doi.org/10.1002/2014GL060868

Sessions, A. L., & Hayes, J. M. (2005). Calculation of hydrogen isotopic fractionations in biogeochemical systems. *Geochimica et Cosmochimica Acta*, *69*(3), 593–597. https://doi.org/10.1016/j.gca.2004.08.005

Smith, F. A., & Freeman, K. H. (2006). Influence of physiology and climate on δD of leaf wax *n*-alkanes from C3 and C4 grasses. *Geochimica et Cosmochimica Acta*, *70*(5), 1172–1187. https://doi.org/10.1016/j.gca.2005.11.006

Sniderman, J. M. K., Brown, J. R., Woodhead, J. D., King, A. D., Gillett, N. P., Tokarska, K. B., et al. (2019). Southern Hemisphere subtropical drying as a transient response to warming. *Nature Climate Change*, *9*, 232–236. https://doi.org/10.1038/s41558-019-0397-9

Stringer, L. C., Dyer, J. C., Reed, M. S., Dougill, A. J., Twyman, C., & Mkwambisi, D. (2009). Adaptations to climate change, drought and desertification: Local insights to enhance policy in southern Africa. *Environmental Science & Policy*, *12*(7), 748–765. https://doi.org/10.1016/j.envsci.2009.04.002

Taylor, A. K., Berke, M. A., Castañeda, I. S., Koutsodendris, A., Campos, H., Hall, I. R., et al. (2021). Plio-Pleistocene continental hydroclimate and Indian Ocean sea surface temperatures at the southeast African margin. *Paleoceanography and Paleoclimatology*, *36*(3), e2020PA004186. https://doi.org/10.1029/2020PA004186

Thoithi, W., Blamey, R. C., & Reason, C. J. C. (2021). Dry spells, wet days, and their trends across Southern Africa during the summer rainy season. *Geophysical Research Letters*, *48*(5), e2020GL091041. https://doi.org/10.1029/2020GL091041

Tierney, J. E., Pausata, F. S., & De Menocal, P. B. (2017). Rainfall regimes of the Green Sahara. *Science Advances*, *3*(1), 1–10. https://doi.org/10.1126/sciadv.1601503

Tipple, B. J., Berke, M. A., Hambach, B., Roden, J. S., & Ehleringer, J. R. (2015). Predicting leaf wax *n*-alkane $^2H/^1H$ ratios: Controlled water source and humidity experiments with hydroponically grown trees confirm predictions of Craig–Gordon model. *Plant, Cell and Environment*, *38*(6), 1035–1047. https://doi.org/10.1111/pce.12457

Tyson, P., & Seely, M. (1980). Local winds over the central Namib. *South African Geographical Journal*, *62*(2), 135–150. https://doi.org/10.1080/03736245.1980.10559630

Vogts, A., Badewien, T., Rullkötter, J., & Schefuß, E. (2016). Near-constant apparent hydrogen isotope fractionation between leaf wax *n*-alkanes and precipitation in tropical regions: Evidence from a marine sediment transect off SW Africa. *Organic Geochemistry*, *96*, 18–27. https://doi.org/10.1016/j.orggeochem.2016.03.003

Wu, Z., & Huang, N. E. (2004). A study of the characteristics of white noise using the empirical mode decomposition method. *Proceedings of the Royal Society A: Mathematical, Physical and Engineering Sciences*, *460*(2046), 1597–1611. https://doi.org/10.1098/rspa.2003.1221

Xie, S. P., Deser, C., Vecchi, G. A., Ma, J., Teng, H., & Wittenberg, A. T. (2010). Global warming pattern formation: Sea surface temperature and rainfall. *Journal of Climate*, *23*(4), 966–986. https://doi.org/10.1175/2009JCLI3329.1

Zhao, X., Koutsodendris, A., Caley, T., & Dupont, L. (2020). Hydroclimate change in subtropical South Africa during the mid-Piacenzian Warm Period. *Quaternary Science Reviews*, *249*, 106643. https://doi.org/10.1016/j.quascirev.2020.106643